Relative intensities of $2s^2 2p^k$-$2s\,2p^{k+1}$ transitions in F I— to B I—like Ti, Cr, Fe, Ni, and Ge in a tokamak plasma: A comparison of experiment and theory

B. C. Stratton* and H. W. Moos
Department of Physics and Astronomy, The Johns Hopkins University, Baltimore, Maryland 21218

S. Suckewer
Plasma Physics Laboratory, Princeton University, Princeton, New Jersey 08544

U. Feldman and J. F. Seely
E. O. Hulburt Center for Space Research, Naval Research Laboratory, Washington, D.C. 20375

A. K. Bhatia
Laboratory for Astronomy and Astrophysics, Goddard Space Flight Center, National Aeronautics and Space Administration, Greenbelt, Maryland 20771
(Received 21 November 1984)

Measured relative intensities of a number of allowed $2s^2 2p^k$-$2s\,2p^{k+1}$ transitions (60—200 Å) in the F I— to B I—like ions of titanium, chromium, iron, nickel, and germanium are compared with values from level-population calculations. The measurements are from Princeton Large Torus (PLT) tokamak plasmas with electron densities of $\sim 2.5\times 10^{13}$ cm^{-3}. For titanium and chromium, data from plasmas with densities of $\sim 5\times 10^{12}$ cm^{-3} are also presented; a number of density-dependent line-intensity ratios are found. The spectra were obtained with use of a grazing-incidence time-resolving spectrograph which was radiometrically calibrated with use of synchrotron radiation from the National Bureau of Standards Synchrotron Ultraviolet Radiation Facility (SURF II). The measured relative intensities are therefore reliable. For the majority of the observed lines, agreement between the measured and calculated relative intensities is within 30%, the estimated accuracy of the measurements; significant discrepancies are found in the titanium ions at the low density. The discrepancies, some of which are due to blends, are discussed. Thus, the level-population calculations may be used with some confidence for spectroscopic plasma diagnostics. In the C I—like ions, there is some evidence that calculations which include proton-collisional excitation and deexcitation between the levels of the ground configuration are in better agreement with the measurements than those that do not, indicating that proton collisions should be included in the calculations for these ions.

I. INTRODUCTION

Allowed $2s^2 2p^k$-$2s\,2p^{k+1}$ transitions in the F I— to B I—like ions of elements with $Z \geq 20$ are often observed in spectra of high-temperature ($T_e \approx 1$ keV) laboratory and astrophysical plasmas, for example, tokamak[1–4] and solar-flare[5] plasmas. The lines corresponding to these transitions are primarily emitted at wavelengths below 300 Å.

Calculations of level populations in these ions play an important role in the interpretation of measured line intensities for plasma diagnostics. In particular, the level-population calculations are used in tokamak plasma spectroscopy to derive impurity ion densities and radiated power losses from measurements of line brightnesses. The emission measure of astrophysical sources can be obtained from observations using level-population calculations. Also, the calculations show that the populations of some levels are not proportional to the electron density of the plasma. Line-intensity ratios in which the density dependence is different for the two transitions can therefore be used to make spatially localized measurements of the density. This technique is particularly important for astrophysical plasmas, such as solar flares, for which nonspectroscopic density diagnostics are not available. It could also be used in low-density laboratory plasmas for which other density diagnostics are not feasible or available. In addition, if the level-population calculations are accurate, spectroscopic diagnostics can be reliably performed using observations of a small number of lines; requirements on the spectral coverage and resolution of the instrumentation can therefore be relaxed.

The level-population models, and the atomic data calculations on which they are based, are complex and involve approximations. It is therefore important to experimentally check their accuracy using observed relative intensities of lines from a well-diagnosed laboratory plasma, such as that of a tokamak. This is not possible using astrophysical data because the electron density is not independently known. Level-population calculations in high-Z ions have been checked only for certain transitions in highly ionized iron. Suckewer and Hinnov[1] measured

the intensities of allowed (90—300 Å) and forbidden (800—3000 Å) lines of Fe XVIII, Fe XX, and Fe XXII from Princeton Large Torus (PLT) tokamak plasmas with densities of $(2-3)\times10^{13}$ cm^{-3} and found generally good agreement with their level-population calculations. Stratton, Moos, and Finkenthal[2] used iron spectra from two PLT plasmas with densities of 5×10^{12} and 3.5×10^{13} cm^{-3} to show that intensity ratios of certain allowed lines of Fe XIX—Fe XXII can be reliably used as density diagnostics. While these measurements showed good agreement with the level-population calculations in most cases, it is clearly desirable to extend the comparison to additional transitions and to elements other than iron.

This paper presents a comparison of measured and calculated[6–8] relative intensities of many allowed $2s^22p^k$-$2s\,2p^{k+1}$ transitions (i.e., those allowed by the *LS*-coupling selection rules for electric dipole radiation) in the F I– to B I–like ions of titanium, chromium, iron, nickel, and germanium. With the exception of germanium, these elements are often found as intrinsic impurities in tokamak plasmas. Spectra for all the elements were obtained from PLT tokamak plasmas with electron densities of approximately 2.5×10^{13} cm^{-3}. For titanium and chromium, spectra were also obtained at a density of approximately 5×10^{12} cm^{-3}, which allows the density dependence of the line-intensity ratios in these two elements to be examined. This is by far the most extensive comparison of measured and calculated relative intensities of allowed transitions in these ions to date.

At the high density, good agreement with the level-population calculations is found in most cases. Most of the discrepancies can be reasonably attributed to blending of the lines. However, at the low density, some significant disagreements between the measurements and calculations are found. In the C I–like ions there is some evidence that calculations which include proton-collisional excitation and deexcitation between the levels of the ground configuration are in better agreement with the measurements than those that do not.

An important feature of this survey is that the measurements were made using a grazing-incidence time-resolving spectrograph which has been radiometrically calibrated using synchrotron radiation from the National Bureau of Standards Synchrotron Ultraviolet Radiation Facility (SURF II) electron storage ring. The measured relative intensities are therefore reliable; this is confirmed by a comparison of a number of measured and calculated branching ratios. In addition, the spectrograph is capable of observing an entire spectral region containing many lines during a single discharge; thus, the measured relative intensities are not affected by discharge-to-discharge variations in the plasma parameters.

There are several reasons for using five elements, instead of just one. In these ions many of these lines are blended due to the 0.7-Å spectrograph resolution. Lines that are blended in one element are often unblended in another element; thus, additional transitions can be observed by using several elements. Significant discrepancies between measured and calculated relative intensities can often be resolved by comparing measurements from several elements. If the discrepancy is consistently observed, it is probably due to a problem with the calculations; if it is observed in only one element, it is probably due to a problem with the measurements. Finally, if the same transitions are observed in several elements, the trend in the relative intensities as Z changes can be seen and compared with that predicted by the calculations. For these reasons, it is logical to compare the observed and calculated relative intensities by isoelectronic sequence, rather than by individual element. Also, because the fractional abundances of the ions of a given element are a function of electron temperature, the choice of ion for a particular density measurement depends on the temperature in the plasma region of interest; more possibilities exist if several elements are available.

The lines have been divided into two categories: those whose intensity is proportional to the density (e.g., lines excited from the ground level of the ground configuration) and those whose intensity is not proportional to the density (e.g., lines excited from high-energy levels in the ground configuration). The emphasis in the discussion is on intensity ratios in which one line is from each of these two categories. In addition to their utility as density diagnostics, such ratios provide the most rigorous test of the theory at a given density because the population mechanisms are quite different for the upper levels of the lines involved.

This paper is organized in the following way. Section II gives a brief description of level-population mechanisms in low-density plasmas and of the level-population calculations; experimental details, such as the spectrograph, are discussed in Sec. III; comparison of the measured and calculated relative intensities by isoelectronic sequence is given in Sec. IV; and Sec. V summarizes the results.

II. LEVEL-POPULATION MECHANISMS IN LOW-DENSITY PLASMAS

The brightness B_{ji}(photons/sec cm^2 sr) of the line due to the transition from level j to level i of an ion may be written

$$B_{ji}=\frac{1}{4\pi}\int n_z n_j A_{ji}\,ds\ , \tag{1}$$

where n_z(cm^{-3}) is the density of ions in ionization state z, n_j is the fraction of the total level population of the ion in the upper level j, A_{ji}(sec^{-1}) is the radiative decay rate from level j to level i, and the integration path is the spectrograph line of sight. The total level population of the ion is normalized to unity:

$$\sum_j n_j=1\ , \tag{2}$$

where the summation extends over all levels of the ion.

For $\Delta n=0$ transitions, such as those considered here, n_j depends very weakly on the electron temperature over the range of values in which the emitting ion exists (as discussed below). Thus, provided that n_j does not vary rapidly with electron density over the region in which the ion exists, Eq. (1) can be written to a good approximation as

$$B_{ji}=\frac{1}{4\pi}n_jA_{ji}\int n_z ds\ . \tag{3}$$

For $\Delta n=0$ transitions, the ratio of the brightness of two lines emitted by the same ionization state is therefore the ratio of the values of n_jA_{ji} for the two transitions. Such ratios have the experimental advantage that the absolute value and spatial distribution of n_z do not need to be known; hence, it is not necessary to measure the spatial distribution of the emissions.

In a low-density ($n_e\approx10^{13}$ cm^{-3}), high-temperature ($T_e\approx1$–2 keV) plasma, the important level-population mechanisms are electron-impact excitation and deexcitation and radiative decay. Thus, the level populations are given by the system of equations

$$\frac{dn_j}{dt}=n_e\sum_i n_iC_{ij}-n_e\sum_i n_jC_{ji}+\sum_{i(>j)}n_iA_{ij}-\sum_{i(<j)}n_jA_{ji}\ , \tag{4}$$

where C_{ij} is the electron-impact excitation or deexcitation rate coefficient for the transition from level i to level j. In most cases proton-impact excitation and deexcitation rates are small compared to the electron-collisional rates and may therefore be neglected; exceptions can occur for transitions between levels separated by a small energy difference, such as the levels of a fine-structure multiplet. In these cases proton-collisional rates can be comparable to, or even larger than, the electron-collisional rates and must therefore be included in the level-population equations. Because the proton-collisional rates are important only in specific cases (see Sec. IV D), they are not explicitly shown in Eqs. (4). The level populations respond rapidly to changes in the plasma parameters; a steady-state solution ($dn_j/dt=0$) to Eqs. (4) may therefore be used.

Because it is not feasible to include all levels of an ion in the solution of Eqs.(4), the levels included are restricted to those that are strongly coupled by collisional and radiative transitions to the levels of interest. In the F I– to B I–like ions the ground and first two excited configurations are of the types $2s^22p^k$, $2s\,2p^{k+1}$, and $2p^{k+2}$. The levels of these configurations are strongly coupled and are therefore included in calculations of the intensities of the $2s^22p^k$-$2s\,2p^{k+1}$ transitions. Levels of higher-energy configurations, such as $2s^22p^{k-1}nl$ (where $n\geq3$), can also be included. However, with a few exceptions, the levels of these configurations are not expected to contribute significantly by radiative decay to the populations of the levels of the $2s^22p^k$ and $2s\,2p^{k+1}$ configurations; as a result, they are not included in the level-population model used here. This conclusion is supported by level-population calculations for Fe XX (Ref. 9) and Fe XXII (Ref. 10) which show that including configurations above $2p^{k+2}$ does not significantly affect the populations of the $2s^22p^k$ and $2s\,2p^{k+1}$ levels.

The level-population calculations used here are by Bhatia, Feldman, and Doschek[6] for titanium; Feldman, Doschek, Cheng, and Bhatia[7] for chromium; and Feldman, Seely, and Bhatia[8] for iron, nickel, and germanium. Titanium and chromium level-population calculations at a density near 5×10^{12} cm^{-3} are not available in the literature. These calculations were performed by the authors. In all of these calculations the following procedure was used. The energy levels and wave functions for the levels of the $2s^22p^k$, $2s\,2p^{k+1}$, and $2p^{k+2}$ configurations were calculated in intermediate coupling assuming a nonrelativistic Hamiltonian and interaction between these three configurations; relativistic effects were included as perturbations. The radiative decay rates were calculated from these energy levels and wave functions and are estimated to be accurate to 10–20% for allowed transitions. The distorted-wave approximation including interaction between the same three configurations was used to calculate the electron collision strengths. The electron-collisional rate coefficients were calculated from the collision strengths assuming a Maxwellian distribution of electron energies. Because resonances are neglected in distorted-wave calculations, the collision strengths have an estimated accuracy of a factor of 2. Proton-collisional rate coefficients for transitions between levels of the ground configurations were calculated using a semiclassical technique. The calculations were performed with and without proton collisions between the levels of the ground configuration. In most cases there was little difference between the two sets of calculations; an exception in the C I–like ions is discussed below. More detailed descriptions of the calculations can be found in the above references.

The level populations for titanium[6] and chromium[7] were calculated at several densities; those closest to the higher-density observations are 1.6×10^{13} and 4.0×10^{13} cm^{-3}. The level populations at these two densities were averaged together to provide values at a density of 2.8×10^{13} cm^{-3}. The level populations for these elements were also calculated at a density of 4.0×10^{12} cm^{-3}. For iron, nickel, and germanium, the level-population calculations assumed a density of 2.5×10^{13} cm^{-3}.

The electron-collisional rates for $\Delta n=0$ transitions are insensitive to temperature changes over the range of values in which the ions exist. As seen in Eqs. (4), the only possible temperature dependence of the level populations arises from the collisional transition rates; thus, the intensities of $2s^22p^k$-$2s\,2p^{k+1}$ transitions are insensitive to temperature changes to a good approximation. For each ion, the level-population calculations assumed the temperature of maximum abundance in coronal equilibrium. The temperature independence of these transitions in Fe XVIII–Fe XXII is demonstrated by level-population calculations[7,10–12] covering a range of temperatures around the coronal equilibrium value. Intensity ratios of these transitions are well suited for density diagnostics because they are not complicated by an additional dependence on the temperature. Conversely, interpretation of the tokamak measurements is simplified because it is not necessary to know the spatial distribution, and the corresponding temperature, of the emitting ions.

The reasons for the density dependence of line-intensity ratios are given in detail elsewhere;[13–15] the present discussion is therefore brief. Density-dependent intensity ratios of $2s^22p^k$-$2s\,2p^{k+1}$ transitions occur when one of the lines is excited directly from the ground level, while the other is primarily excited in two steps: from the ground

level to an excited level in the ground configuration and then to a level of an excited configuration. Thus, the intensity of the first line is proportional to n_e and, because two excitations are required, the intensity of the second line is proportional to n_e^k, where $k>1$. The ratio of line intensities is therefore density dependent. The utility of these ratios as density diagnostics is limited at low density by the low intensity of the line from the level populated from the excited level of the ground configuration; at high density, the level populations in the ground configuration approach Boltzmann equilibrium and therefore depend very weakly on the density. For transitions in the F I– to B I–like iron ions, the density-sensitive range is typically one or two orders of magnitude in the 10^{11}–10^{15} cm^{-3} region. Because the levels of the ground configuration tend to become farther separated as the Z of the emitting ion increases, Boltzmann equilibrium between them is reached at higher density. Thus, the density-sensitive region for a given line-intensity ratio shifts to higher density as Z increases.

III. EXPERIMENTAL ARRANGEMENT

The PLT tokamak produces plasmas with central electron densities up to 1×10^{14} cm^{-3} and central electron temperatures up to 2.0 keV in Ohmically heated discharges. Ohmically heated plasmas typically have a duration of approximately 1 sec. Detailed descriptions of PLT plasmas may be found elsewhere.[16]

The temperature radial distribution is centrally peaked during the current plateau period of the discharge. As a result of the temperature gradient, different ionization states of an impurity element exist at different distances from the center of the plasma. Measurements[1] of the radial distributions of emissions from Fe XVIII–Fe XXIV show that due to radial particle transport, these ions exist in PLT plasmas at temperatures higher than the coronal equilibrium values, close to their ionization potentials. However, because the level populations depend very weakly on temperature, comparison of measured line-intensity ratios with those calculated assuming temperatures of maximum fractional abundance in coronal equilibrium is valid.

The line-average electron density ($\bar{n}_e$) was measured by a 2-mm-microwave interferometer which views a line of sight through the center of the plasma. These measurements have an accuracy of approximately 10%. Because the density radial distribution is centrally peaked, the density at the location of a given ion near the plasma center may be greater than $\bar{n}_e$ by as much as 50%. The high-density observations were made at values of $\bar{n}_e$ ranging from 1.4×10^{13} to 2.5×10^{13} cm^{-3}; thus, the density in the region where the observed ions exist was approximately $(2.0$–$3.0)\times10^{13}$ cm^{-3}. The low-density observations were made at $\bar{n}_e=4\times10^{12}$ cm^{-3} for titanium and $\bar{n}_e=5\times10^{12}$ cm^{-3} for chromium. Level-population[6,7] calculations at different densities show that the intensities of the observed lines are not sufficiently density sensitive to make closer agreement between the densities of the observations and calculations necessary.

The spectrograph is a 1-m time-resolving grazing-incidence instrument (described in detail elsewhere[17]) which viewed the PLT plasma along a line of sight passing through the minor axis of the torus. Overall wavelength coverage is 15–360 Å. The detector is an image intensifier tube consisting of a funneled MgF_2-coated microchannel plate with a P-20 phosphor screen behind it; a fiber optics bundle connects the phosphor to a 1024 element (pixel) photodiode array. The photodiode array integrates the signal for a selected period of time; an integration time of 5.4 msec was used in the present experiment. The detector can be moved along the Rowland circle in order to observe different wavelength regions; with the detector centered at 100 Å, a region approximately 60 Å wide can be observed during a single discharge. The spectral resolution is approximately 0.7 Å (line profile full width at half maximum). A wavelength calibration was performed using well-known lines from intrinsic (carbon, oxygen, titanium, and iron) and injected impurities in the tokamak plasma; the wavelength of an unknown line can be measured to ±0.2 Å. The radiometric calibration extends from 60 to 360 Å.

Small amounts of the impurity elements were injected into the current-plateau period of Ohmically heated deuterium discharges using the laser-blowoff method.[18,19] Typical decay times for emissions from the F I– to B I–like ions were 20 msec or longer; the line brightnesses did not change substantially during one detector integration time.

IV. COMPARISON OF MEASURED AND CALCULATED RELATIVE INTENSITIES

For each element, a spectrum of the wavelength region most populated with lines is shown in Figs. 1–5. The measured line-average electron density in each case is given. The lines were identified on the basis of the agreement between the measured wavelengths and published values, the relative intensities of the lines, and their time evolutions. Each line was checked for blending with lines of the injected element and of intrinsic impurities. For blended lines, the identifications given in the figures are for the line considered to be the strongest; if both components are of approximately equal intensity, the peak is labeled with both identifications.

For titanium, chromium, iron, and nickel, the wavelengths are from Lawson, Peacock, and Stamp.[20] The wavelengths of Edlén[21,22] are used for the Ge XXIV and Ge XXV lines. For the Ge XXVI and Ge XXVII lines, the wavelengths are those of Behring *et al.*[23] The Ge XXVIII lines have not been previously observed and are identified for the first time in the present work. These identifications are based primarily on the good agreement between the measured wavelengths and the predictions of Edlén[24] and the relative intensities. The measured wavelengths, which have an estimated accuracy of ±0.2 Å, are given in Fig. 5.

The peak brightness after injection of each line was measured and converted to a relative intensity by taking its ratio with the brightness of a line due to a transition observed in all five elements. Where possible, this reference line was chosen to be strong and unblended. The

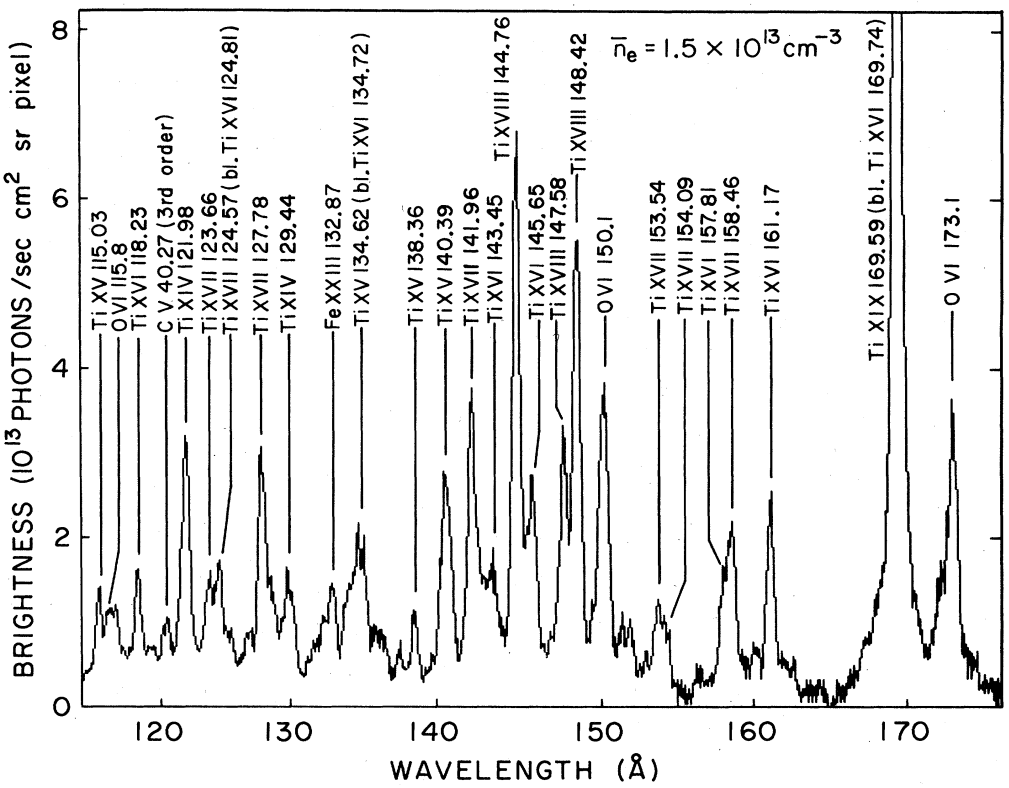

FIG. 1. Titanium spectrum in the 115—175-Å region. Bandpass per picture element ("pixel") at the center of the detector is 0.07 Å/pixel.

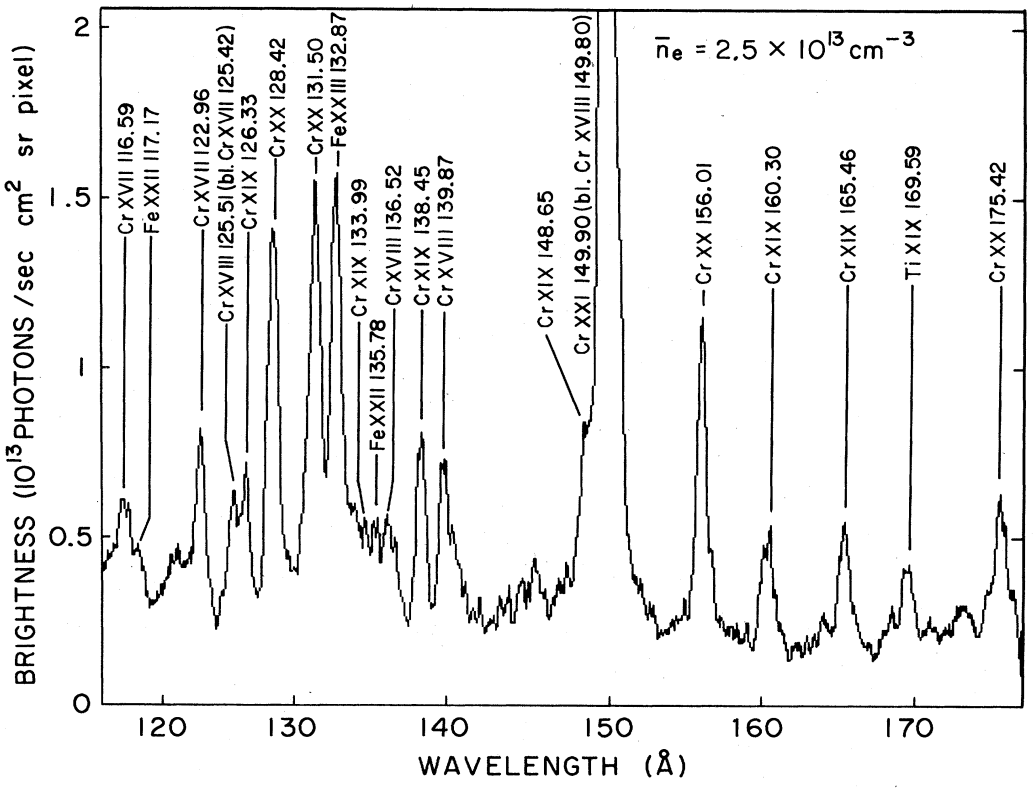

FIG. 2. Chromium spectrum in the 115—175-Å region. Bandpass per pixel at the center of the detector is 0.07 Å/pixel.

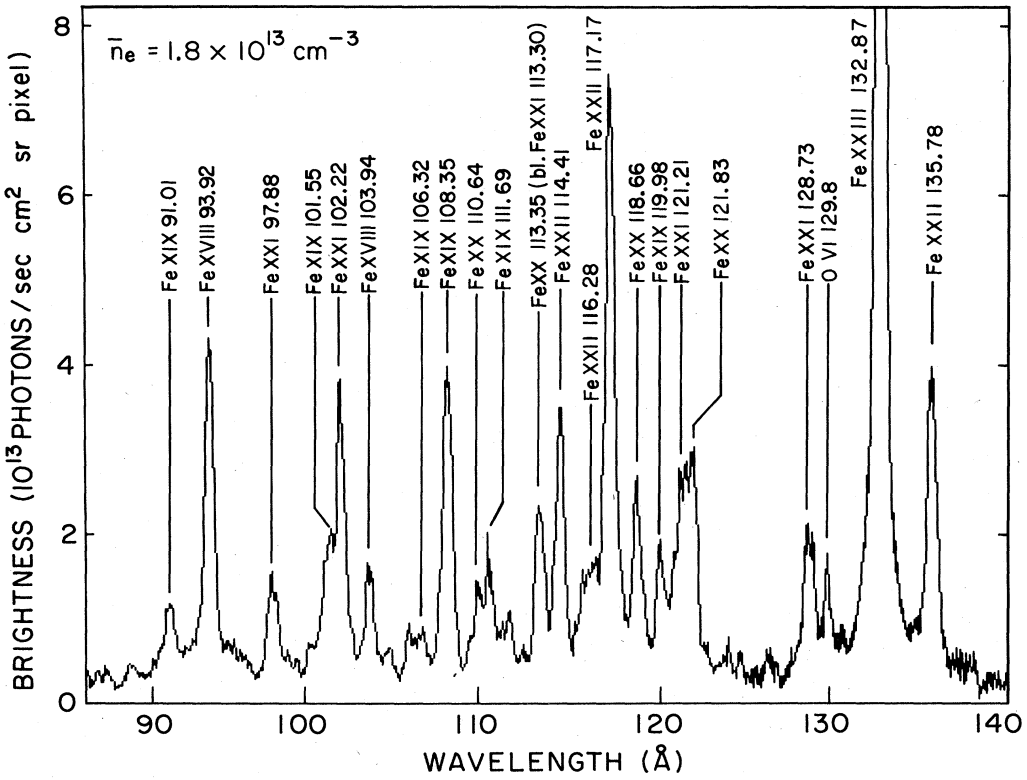

FIG. 3. Iron spectrum in the 85—140-Å region. Bandpass per pixel at the center of the detector is 0.06 Å/pixel.

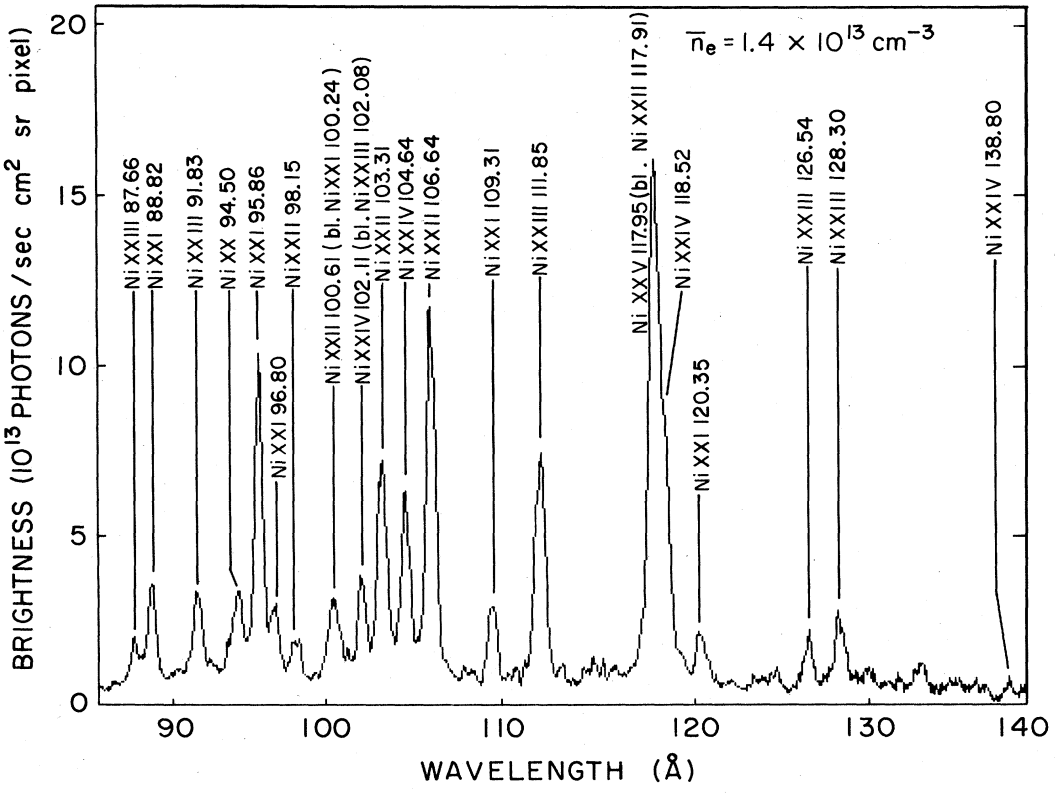

FIG. 4. Nickel spectrum in the 85—140-Å region. Bandpass per pixel at the center of the detector is 0.06 Å/pixel.

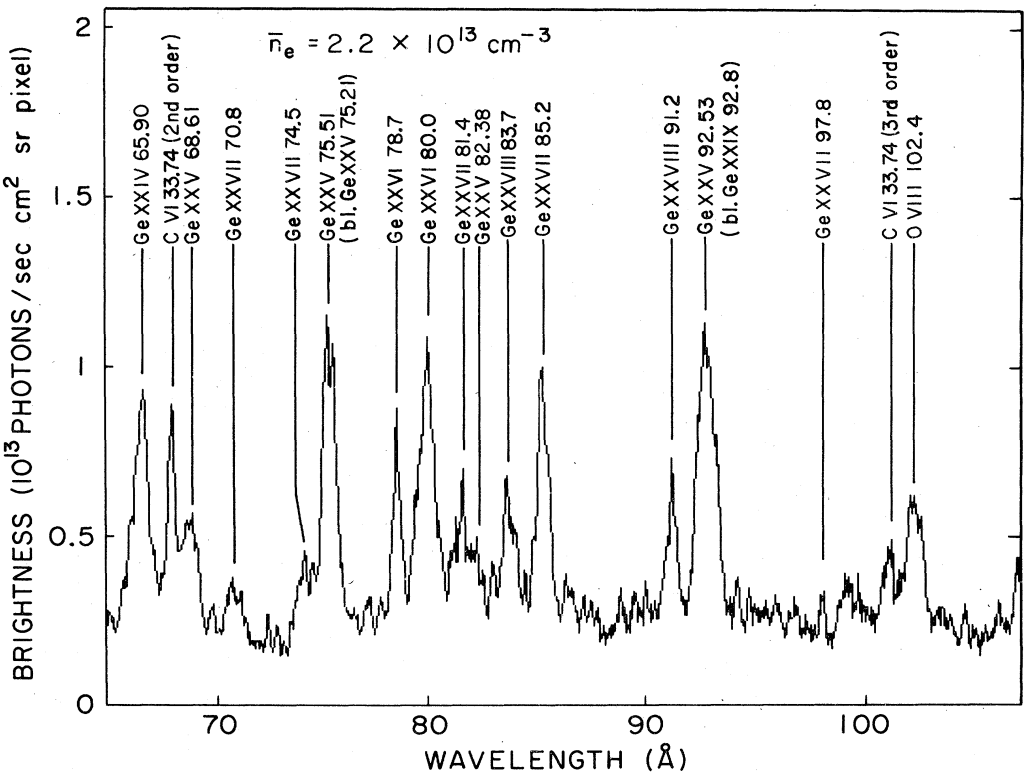

FIG. 5. Germanium spectrum in the 65—105-Å region. Bandpass per pixel at the center of the detector is 0.05 Å/pixel.

brightness of each line was obtained by integrating over the line profile and subtracting an appropriate background level; the background is primarily due to unresolved weak lines, scattered light in the spectrograph, and continuum radiation. Note that, as a result of the integration, these brightnesses have units of photons/sec cm^2 sr, whereas the vertical axes of Figs. 1—5 have units of photons/sec cm^2 sr pixel. To facilitate approximate conversions between these units, the bandpass per picture element ("pixel") (Å/pixel) at the center of the detector is given in each figure caption. The brightnesses were in the 10^{13}—10^{15} photon sec^{-1} cm^{-2} sr^{-1} range. The observed and calculated branching ratios in the F I—, O I—, and C I—like ions are given in Tables I(a)—I(c). The observed and calculated relative intensities of the lines from the O I— to B I—like ions are listed by isoelectronic sequence in Tables II—V. The wavelengths given in the tables are from the same sources as those in the figures. Not all of the measured relative intensities were taken from the spectra shown in Figs. 1—5. Other spectra obtained under the same conditions were used for the lines outside the wavelength regions shown in the figures and, in some cases, blends with intrinsic impurity lines could be better resolved in other spectra. In the case of two lines widely separated in wavelength, data from adjacent spectral regions were used; the intensity ratio of the two lines was found by normalizing their brightnesses to the brightness of a line from the same ion and common to both spectral regions. This procedure eliminated reproducibility problems caused by comparison of data from different discharges.

The following conventions are used in Tables I—V. Transitions whose intensities are almost proportional to the density are denoted by "P" in the transition column; those whose intensities are not proportional to the density are denoted by "NP." These classifications were made by comparing the calculated level populations for nickel[7] at densities of 1.6×10^{13} and 1×10^{14} cm^{-3}. However, it should be noted that the density range over which the population of a given level is nonlinear varies with Z. Thus, in some elements the nonlinearity is not very strong over the density range considered here. The intensity of the reference line is given as 1. If a line was observed, but was blended with a line of comparable or greater brightness according to the level-population calculations, no measured relative intensity is given and the notation "bl." appears. (In the branching ratios of Table I, "bl." means that one or both of the lines was strongly blended.) Where the level-population calculations show that one of the lines in a blend is much weaker than the other, the relative intensity of the stronger line is given and the blend is noted. Some lines were not observed because their brightnesses were smaller than the minimum observable value; for these lines, the measured relative intensity is listed as zero. Occasionally, the brightness of a line is uncertain because it is weak or poorly separated from another line; in these cases the symbol "$\sim$" is used to indicate that the measured relative intensity is approximate and can be uncertain by as much as a factor of 2. Finally, no listing for the measured relative intensity of a line indi-

TABLE I. (a) $2s^22p^5$-$2s\,2p^6$ branching ratios in the F I–like ions. (b) $2s^22p^4$-$2s\,2p^5$ branching ratios in the O I–like ions. (c) $2s^22p^2$-$2s\,2p^3$ branching ratios in the C I–like ions. [Wavelengths are in Å, from Refs. 20, 22, and 23; (bl.) one or both lines is strongly blended; calculated values in parentheses.]

(a)

	$_{22}$Ti XIV		$_{24}$Cr XVI		$_{26}$Fe XVIII		$_{28}$Ni XX		$_{32}$Ge XXIV	
Ratio	λ	Ratio	λ	Ratio	λ	Ratio	λ	Ratio	λ	Ratio
$^2P_{1/2}$-$^2S_{1/2}$ / $^2P_{3/2}$-$^2S_{1/2}$	129.44 / 121.98	0.50 (0.42)	115.53 / 106.63	0.31 (0.40)	103.94 / 93.92[a]	0.31 (0.38)	94.50 / 83.18	0.38 (0.34)	79.75[b] / 65.90	bl. (0.27)

(b)

	$_{22}$Ti XV		$_{24}$Cr XVII		$_{26}$Fe XIX		$_{28}$Ni XXI		$_{32}$Ge XXV	
Ratio	λ	Ratio	λ	Ratio	λ	Ratio	λ	Ratio	λ	Ratio
$^3P_1$-$^3P_1$ / $^3P_2$-$^3P_1$	142.13 / 134.62	bl. (0.52)	125.42 / 116.59	bl. (0.43)	111.69 / 101.55	~0.76 (0.39)	100.24 / 88.82	bl. (0.36)	82.39 / 68.60	0.28 (0.24)
$^3P_0$-$^3P_1$ / $^3P_2$-$^3P_1$	142.74 / 134.62	bl. (0.67)	125.06 / 116.59	bl. (0.54)	109.95 / 101.55	bl. (0.51)	96.83 / 88.82	0.82 (0.51)	75.17 / 68.60	bl. (0.42)
$^3P_1$-$^3P_2$ / $^3P_2$-$^3P_2$	148.59 / 140.39	bl. (0.29)	132.83 / 122.96	bl. (0.28)	119.98 / 108.35	0.33 (0.27)	109.31 / 95.86	0.25 (0.25)	92.64[c] / 75.51	bl. (0.22)

(c)

	$_{22}$Ti XVII		$_{24}$Cr XIX		$_{26}$Fe XXI		$_{28}$Ni XXIII		$_{32}$Ge XXVII	
Ratio	λ	Ratio	λ	Ratio	λ	Ratio	λ	Ratio	λ	Ratio
$^3P_1$-$^3S_1$ / $^3P_2$-$^3S_1$	123.66 / 127.78	0.39 (0.49)	109.64 / 113.97	(0.45)	97.88[d] / 102.22	0.27 (0.44)	87.66 / 91.83	0.38 (0.37)	70.79 / 74.29	(0.31)

[a]bl. $_{26}$Fe XX 93.79 Å.
[b]bl. $_{32}$Ge XXVI 80.0 Å.
[c]bl. $_{32}$Ge XXVI 92.69 Å.
[d]bl. $_{26}$Fe XX 98.37 Å.

TABLE II. Relative intensities of $2s^22p^4$-$2s\,2p^5$ transitions in O I–like ions. [Wavelengths in Å, from Refs. 20 and 22; (P) intensity approximately proportional to n_e; (NP) intensity not proportional to n_e; (H) $n_e \approx 2.5\times10^{13}$ cm^{-3}; (L) $n_e \approx 5\times10^{12}$ cm^{-3}; (bl.) strongly blended line; calculated values in parentheses.]

		$_{22}$Ti XV			$_{24}$Cr XVII			$_{26}$Fe XIX			$_{28}$Ni XXI			$_{32}$Ge XXV	
Transition	λ	H	L	λ	H	L	λ	H	λ	H	λ	H	λ	H
$^1D_2$-$^1P_1$ NP	115.03	~0.38 (0.52)	~0.24 (0.20)	101.93	(0.32)	bl. (0.14)	91.02[a]	0.20 (0.24)	81.70	bl. (0.14)	66.38	0 (0.09)
$^3P_2$-$^3P_1$ P	134.62[b]	bl. (0.33)	0.33 (0.34)	116.59	0.40 (0.37)	~0.45 (0.35)	101.55	0.37 (0.41)	88.82	0.33 (0.41)	68.61	0.36 (0.48)
$^3P_1$-$^3P_0$ NP	138.36	0.24 (0.22)	0.27 (0.20)	120.89	bl. (0.17)	0.18 (0.10)	106.32	0.16 (0.13)	93.92	0 (0.05)	73.89	0 (0.007)
$^3P_2$-$^3P_2$ P	140.39	1 (1)	1 (1)	122.96	1 (1)	1 (1)	108.35	1 (1)	95.86[c]	1 (1)	75.51[d]	1 (1)
$^3P_1$-$^3P_1$ P	142.13	bl. (0.17)	bl. (0.17)	125.42	bl. (0.16)	bl. (0.15)	111.69	~0.28 (0.16)	100.24	bl. (0.14)	82.38	~0.10 (0.12)
$^3P_0$-$^3P_1$ P	142.74	bl. (0.22)	~0.27 (0.21)	125.06	bl. (0.20)	bl. (0.20)	109.95	bl. (0.21)	96.83	0.27 (0.21)	75.21	bl. (0.20)
$^3P_1$-$^3P_2$ P	148.59	bl. (0.29)	bl. (0.29)	132.83	bl. (0.28)	bl. (0.28)	119.98	0.33 (0.27)	109.31	0.25 (0.25)	92.53	bl. (0.22)

[a]bl. $_{26}$Fe XXI 91.28 Å.
[b]bl. $_{22}$Ti XV 134.72 Å.
[c]bl. $_{28}$Ni XXII 95.96 Å.
[d]bl. $_{32}$Ge XXV 75.21 Å.

TABLE III. Relative intensities of $2s^22p^3$-$2s\,2p^4$ transitions in N I—like ions. [Wavelengths in Å, from Refs. 20 and 23; (P) intensity approximately proportional to n_e; (NP) intensity not proportional to n_e; (H) $n_e \sim 2.5\times10^{13}$ cm^{-3}; (L) $n_e \approx 5\times10^{12}$ cm^{-3}; (bl.) strongly blended line; calculated values in parentheses.]

		$_{22}$Ti XVI		$_{24}$Cr XVIII			$_{26}$Fe XX		$_{28}$Ni XXII		$_{32}$Ge XXVI	
Transition	λ	*H*	*L*	λ	*H*	*L*	λ	*H*	λ	*H*	λ	*H*
$^2D_{5/2}$-$^2P_{3/2}$ NP	118.23	0.71	0.99	104.98			93.79	bl.	84.07		67.82	bl.
		(0.76)	(0.24)		(0.40)	(0.18)		(0.30)		(0.14)		(0.07)
$^2D_{3/2}$-$^2D_{3/2}$ NP	143.45	~0.77	~0.78	125.51	bl.	bl.	110.64	~0.38	98.15	bl.	78.59	bl.
		(0.51)	(0.16)		(0.32)	(0.08)		(0.23)		(0.07)		(0.07)
$^2D_{5/2}$-$^2D_{5/2}$ NP	145.65	1.28	~1.08	128.10	bl.	bl.	113.35	bl.	100.61	bl.	79.63	bl.
		(0.75)	(0.22)		(0.37)	(0.15)		(0.23)		(0.11)		(0.01)
$^4S_{3/2}$-$^4P_{1/2}$ P	157.81	0.61	0.76	136.52	0.53	0.40	118.66[a]	0.91	103.31[b]	0.59	78.69	0.39
		(0.51)	(0.51)		(0.52)	(0.53)		(0.52)		(0.46)		(0.40)
$^4S_{3/2}$-$^4P_{3/2}$ P	161.17	1	1	139.87	1	1	121.83	~1	106.04[c]	1	80.08[d]	1
		(1)	(1)		(1)	(1)		(1)		(1)		(1)

[a]bl. $_{26}$Fe XXI 118.69 Å.
[b]bl. $_{28}$Ni XXIII 103.23 Å.
[c]bl. $_{28}$Ni XXIII 106.02 Å.
[d]bl. $_{32}$Ge XXIV 79.78 Å.

cates that the line was not observed due to a lack of quality data at the appropriate wavelength and density.

Figures 6—10 are scatter plots which show the degree of agreement between the measured and calculated branching ratios and relative intensities in the O I— to B I—like ions. In each case the diagonal line indicates perfect agreement between the measured and calculated values. The open circles refer to the high-density data and the solid points to the low-density data.

A. Branching ratios

Tables I(a)—I(c) list the observed and calculated branching ratios in the F I—, O I—, and C I—like ions, respective-

TABLE IV. Relative intensities of $2s^22p^2$-$2s\,2p^3$ transitions in C I—like ions. [Wavelengths in Å, from Refs. 8, 20, and 23; (P) intensity approximately proportional to n_e; (NP) intensity not proportional to n_e; (H) $n_e \sim 2.5\times10^{13}$ cm^{-3}; (L) $n_e \sim 5\times10^{12}$ cm^{-3}; (bl.) strongly blended line; calculated values in parentheses; values not including proton collisions in square brackets.]

		$_{22}$Ti XVII		$_{24}$Cr XIX			$_{26}$Fe XXI		$_{28}$Ni XXIII		$_{32}$Ge XXVII	
Transition	λ	*H*	*L*	λ	*H*	*L*	λ	*H*	λ	*H*	λ	*H*
$^3P_1$-$^3S_1$ P	123.66	0.54	1.81	109.64			97.88[a]	0.85	87.66[b]	0.44	70.79	~1.00
		(0.45)	(0.51)		(0.43)	(0.60)		(0.68)		(0.71)		(0.68)
$^3P_2$-$^3S_1$ P	127.78	1.29	1.69	113.97	0.95		102.22	~3.12	91.83	1.16	74.29	bl.
		(0.91)	(1.01)		(0.95)	(1.34)		(1.56)		(1.91)		(2.20)
$^1D_2$-$^1D_2$ NP	141.96[c]	1.88	1.93	126.33[d]	~1.77	bl.	113.30	bl.	102.08	bl.	83.04	bl.
		(0.76)	(0.40)		(0.50)	(0.33)		(0.54)		(0.30)		(0.24)
$^3P_1$-$^3P_1$ P	153.54	~0.45	bl.	133.99	bl.	0.72	117.51	bl.	103.23	bl.	80.06[e]	bl.
		(0.39)	(0.46)		(0.38)	(0.72)		(0.83)		(1.00)		(0.90)
$^3P_1$-$^3P_0$ NP	154.09	~0.26	bl.	134.89	bl.	~0.50	118.69	bl.	104.70	bl.	82.03[e]	bl.
		(0.26)	(0.30)		(0.22)	(0.29)		(0.36)		(0.21)		(0.04)
$^3P_2$-$^3P_2$ NP	158.46	~0.75	~2.40	138.45	1.48	1.17	121.21	~1.30	106.02	bl.	81.37	~3.30
		(1.01)	(1.07)		(1.05)	(1.18)		(1.33)		(1.64)		(2.20)
$^3P_0$-$^3D_1$ NP	172.22	bl.	bl.	148.65	bl.	1.73	128.73	1.65	111.85	3.24	85.18	5.2
		(0.42)	(0.68)		(0.57)	(1.67)		(1.94)		(4.72)		(10.80)
								[2.05]		[6.32]		[25.00]
$^3P_1$-$^3D_2$ NP	182.06[f]	~1.54	~0.67	160.30	1.11	0.73	142.16	1.50	126.54	0.72	100.96[e]	0
		(0.93)	(1.11)		(0.81)	(1.15)		(1.39)		(0.78)		(0.22)
$^3P_2$-$^3D_3$ NP	188.31	1	1	165.40	1	1	145.65	1	128.30	1	97.83	1
		(1)	(1)		(1)	(1)		(1)		(1)		(1)

[a]bl. $_{26}$Fe XX 98.37 Å.
[b]bl. $_{28}$Ni XXIV 87.50 Å.
[c]bl. $_{22}$Ti XV 142.13 Å.
[d]bl. $_{24}$Cr XIX 126.30 Å.
[e]Predicted wavelength (Ref. 8).
[f]bl. $_6$C VI 182.10 Å.

TABLE V. Relative intensities of $2s^22p$-$2s\,2p^2$ transitions in B I—like ions. [Wavelengths in Å, from Refs. 20 and 24; (P) intensity approximately proportional to n_e; (NP) intensity not proportional to n_e; (H) $n_e \approx 2.5\times10^{13}$ cm^{-3}; (L) $n_e \approx 5\times10^{12}$ cm^{-3}; (bl.) strongly blended line; calculated values in parentheses.]

Transition	$_{22}$Ti XVIII λ	*H*	*L*	$_{24}$Cr XX λ	*H*	*L*	$_{26}$Fe XXII λ	*H*	$_{28}$Ni XXIV λ	*H*	$_{32}$Ge XXVIII λ	*H*
$^2P_{3/2}$-$^2P_{3/2}$ P	144.76	1.30	0.85	128.42[a]	0.78	1.00	114.41	0.40	102.11	bl.	81.37[b]	bl.
		(1.52)	(0.99)		(0.86)	(0.46)		(0.56)		(0.20)		(0.09)
$^2P_{3/2}$-$^2P_{1/2}$ NP	147.58	0.61	~0.24	130.76	bl.	bl.	116.28	~0.20	103.53	bl.	82.6[b]	0
		(0.65)	(0.43)		(0.35)	(0.18)		(0.21)		(0.06)		(0.01)
$^2P_{1/2}$-$^2S_{1/2}$ P	148.42	1	1	131.50	1	1	117.17[c]	1	104.64	1	83.7	1
		(1)	(1)		(1)	(1)		(1)		(1)		(1)
$^2P_{1/2}$-$^2D_{3/2}$ P	179.87	1.19	0.59	156.01	0.67	1.00	135.78	0.49	118.52	bl.	91.2	1.37
		(1.00)	(0.97)		(0.95)	(0.93)		(0.90)		(0.88)		(0.95)
$^2P_{3/2}$-$^2D_{5/2}$ NP	197.83	0.95	~0.40	175.42	0.32		155.92	0.29	138.80	~0.10	109.04[b]	0
		(1.02)	(0.59)		(0.48)	(0.19)		(0.26)		(0.05)		(0.005)

[a]bl. $_{24}$Cr XVIII 128.10 Å.
[b]Predicted wavelength (Ref. 24).
[c]bl. $_{26}$Fe XXI 117.51 Å.

ly, and Fig. 6 shows the agreement between them. The observations are from the high-density discharges. In these pairs both lines have a common upper level; the ratio of their intensities is therefore just the ratio of the radiative decay rates. The radiative decay rates for strong allowed transitions in the F I— to B I—like ions are estimated to be accurate to 10—20%.[6,7] Thus, comparison of the measured and calculated branching ratios indicates the reliability of the measured relative intensities of the lines. As seen in the tables, agreement is 30% or better for 10 out of the 12 observed branching ratios; the two cases which show significant disagreement are discussed below. The measured branching ratios in $_{22}$Ti XIV and $_{24}$Cr XVI at the low density are also in good agreement with the calculated values; however, the measured $_{22}$Ti XVII branching ratio at the low density is a factor of 2 larger than the calculated value. As a result of this comparison, the accuracy of the observed relative intensities is conservatively estimated to be ±30%; in the following discussion this is taken to be the criterion for agreement between the measured and calculated relative intensities.

The measured and calculated values of the 111.69-Å to 101.55-Å branching ratio in $_{26}$Fe XIX disagree by a factor of 2. This is attributed to the fact that the 111.69-Å line is poorly separated from the $_{26}$Fe XX 110.64-Å line (see Fig. 3); its brightness is therefore uncertain. In the case of the $_{28}$Ni XXI 96.83-Å to 88.82-Å branching ratio, the disagreement is approximately 50%: The 96.83-Å line is poorly separated from the stronger $_{28}$Ni XXI 95.86-Å line, making its brightness unreliable. Note that the $_{26}$Fe XVIII 93.92-Å line is blended with the $_{26}$Fe XX 93.79-Å line, but the agreement of the measured and calculated values of the $_{26}$Fe XVIII 103.94-Å to 93.92-Å branching ratio implies that the 93.79-Å line is relatively weak. The calculated $_{32}$Ge XXIV branching ratio listed in Table I(a) was obtained by interpolation between the values of Cheng, Kim, and Desclaux[25] for $_{30}$Zn XXII and $_{36}$Kr XXVIII.

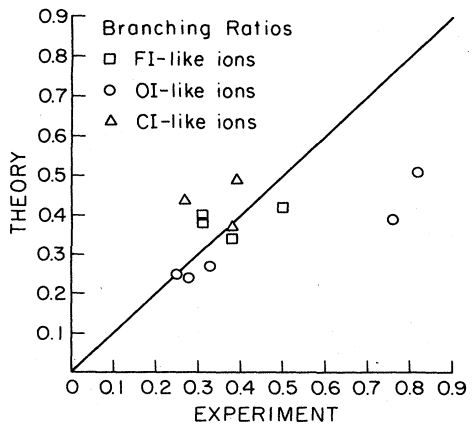

FIG. 6. Comparison between measured and calculated branching ratios. The compared transitions are listed in Table I.

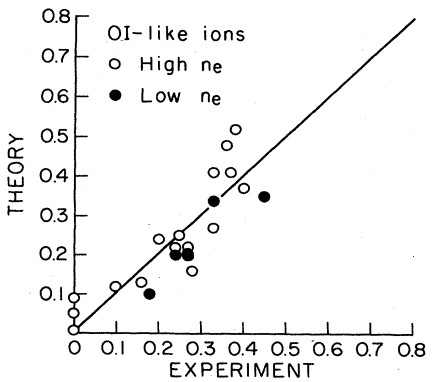

FIG. 7. Comparison of measured and calculated relative intensities in the O I—like ions. The compared transitions are listed in Table II.

B. O I—like ions

The observed $2s^2 2p^4$-$2s\,2p^5$ transitions in the O I—like ions are listed in Table II; the observed and calculated relative intensities of these transitions are compared in Fig. 7. The $^3P_2$-$^3P_2$ reference transition is strong and unblended in all the ions except for $_{32}$Ge XXV 75.51 Å; however, the level-population calculations[8] show that the intensity of the Ge XXV 75.21-Å line with which it is blended is small. Because intersystem electron-collisional and radiative rates are relatively small, the singlet and triplet levels of the $2s\,2p^5$ configuration receive essentially all of their populations from the singlet and triplet levels, respectively, of the $2s^2 2p^4$ configuration. In particular, a comparison of $_{22}$Ti XV collision strengths[6] shows that the $2s\,2p^5\,^1P_1$ level is primarily populated from the $2s^2 2p^4\,^1D_2$ level and the $2s\,2p^5\,^3P_2$ level is primarily populated from the ground $2s^2 2p^4\,^3P_2$ level. Within the $2s^2 2p^4$ configuration, the population of the $^1D_2$ level increases rapidly relative to that of the $^3P_2$ level as the density increases. The $^1D_2$-$^1P_1$ to $^3P_2$-$^3P_2$ intensity ratio is therefore expected to be density dependent; comparison of the measured and calculated values at the two densities shows this to be the case. The observed value of this ratio in $_{22}$Ti XV at the low density and in $_{26}$Fe XIX at the high density is in excellent agreement with the calculated value; in $_{22}$Ti XV at the high density, the observed and calculated values differ by 30%. At a given density, the population of the $2s^2 2p^4\,^1D_2$ level decreases rapidly with increasing Z due to the increasing difference in the energies of the $^1D_2$ and $^3P_2$ levels;[8] as a result, the $^1D_2$-$^1P_1$ transition is too weak to be observed in $_{32}$Ge XXV.

The only observed intensity ratio of ^3P-^3P transitions expected to exhibit an appreciable density dependence is the $^3P_1$-$^3P_0$ to $^3P_2$-$^3P_2$ intensity ratio: The $2s\,2p^5\,^3P_0$ and $2s\,2p^5\,^3P_2$ levels are primarily populated from the widely separated $2s^2 2p^4\,^3P_1$ and $2s^2 2p^4\,^3P_2$ levels, respectively.[7]

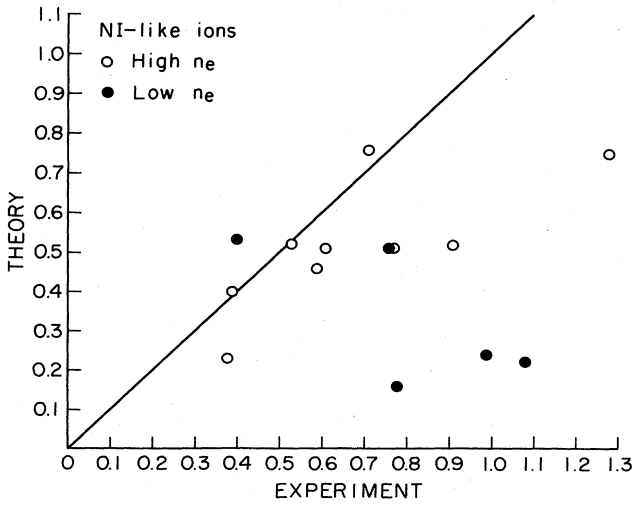

FIG. 8. Comparison of measured and calculated relative intensities in the N I—like ions. The compared transitions are listed in Table III.

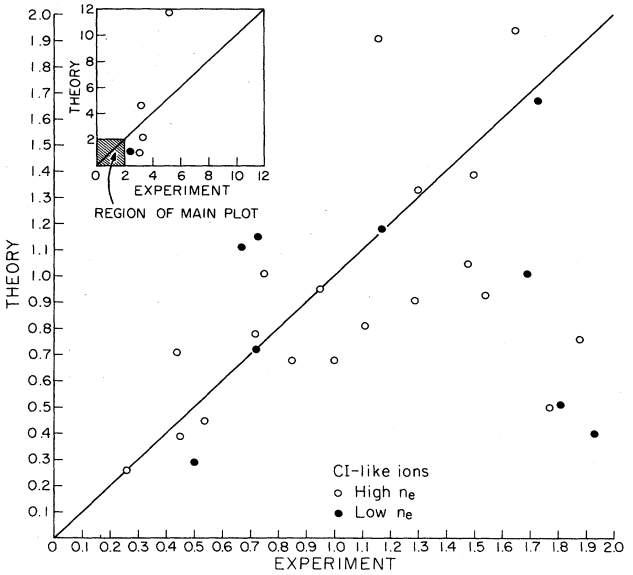

FIG. 9. Comparison of measured and calculated relative intensities in the C I—like ions. Five points not within the range of the main plot are plotted in the inset. The compared transitions are listed in Table IV.

The density sensitivity of this ratio is predicted to increase rapidly with Z over the density range considered here and is very weak for $_2$Ti XV and $_{24}$Cr XVII, as demonstrated by the $_{22}$Ti XV measurements at the two densities. Agreement between the observed and calculated values in $_{22}$Ti XV and $_{26}$Fe XIX at the high density is excellent, but is not as good in $_{22}$Ti XV and $_{24}$Cr XVII at the low density.

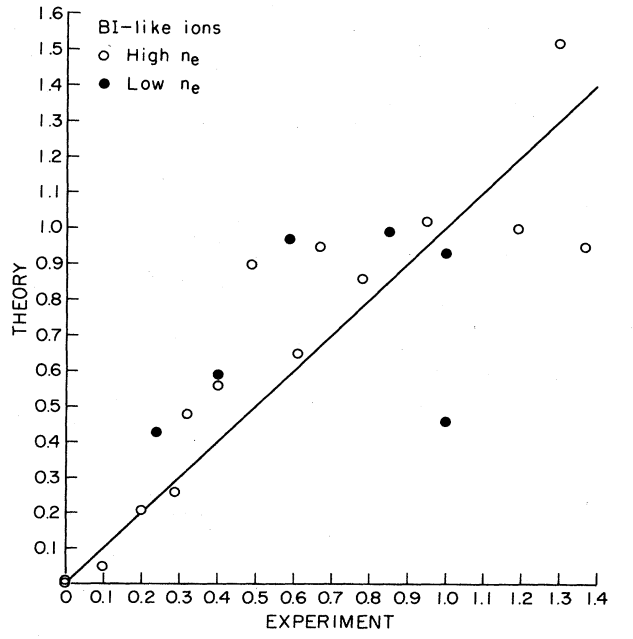

FIG. 10. Comparison of measured and calculated relative intensities in the B I—like ions. The compared transitions are listed in Table V.

This ratio could not be observed in $_{24}$Cr XVII at the high density because the 120.89-Å line was blended with an intrinsic impurity line, probably the third order of C V 40.27 Å. The intensity of the $^3P_1$-$^3P_0$ transition decreases rapidly with increasing Z in the elements above iron;[8] hence, it is not of observable intensity in $_{28}$Ni XXI and $_{32}$Ge XXV.

The upper level of the remaining observed transitions is $2s\,2p^5\,^3P_1$ or $2s\,2p^5\,^3P_2$. The population mechanisms for these levels are similar,[7] so intensity ratios of lines from these levels are not predicted to be density sensitive. With the two exceptions discussed in the preceding subsection, agreement between the measured and calculated relative intensities of transitions from these levels is good, as seen in Table II.

C. N I—like ions

The relative intensities of the observed $2s^2 2p^3$-$2s\,2p^4$ transitions in the N I—like ions are listed in Table III, and the measured and calculated values are compared in Fig. 8. The most intense transition in these ions is $^4S_{3/2}$-$^4P_{5/2}$, but it is blended with the stronger $2s^2\,^1S_0$—$2s\,2p\,^1P_1$ transition is in the Be I—like ions in all the observed elements and is therefore not usable. The strongest of the remaining transitions, $^4S_{3/2}$-$^4P_{3/2}$, is used as the reference transition. The line due to this transition in $_{28}$Ni XXII, 106.04 Å, is blended with the weaker $_{28}$Ni XXIII 106.012-Å line.

The $2s\,2p^4\,^4P$ levels are primarily populated from the only quartet level in the ground configuration, the $^4S_{3/2}$ level.[7] The levels of the doublets in the $2s\,2p^4$ configuration, ^2S, ^2P, and ^2D, receive their populations mainly from the ^2P and ^2D levels of the $2s^2 2p^3$ configuration.[7] Thus, the intensity ratio of a line from a $2s\,2p^4\,^4P$ level with a line from a level of one of the $2s\,2p^4$ doublets should be density sensitive. Several such ratios are found in Table III. In $_{22}$Ti XVI the agreement between the observed and calculated values of these ratios is reasonably good at the high density, but is poor at the low density: the observed lines from the $2s\,2p^4$ doublets are consistently brighter than predicted relative to those from the $2s\,2p^4\,^4P$ levels. As a result of blending and the decrease in the intensities of the lines from the $2s\,2p^4$ doublets with increasing Z, these line-intensity ratios could not be observed in $_{24}$Cr XVIII at either density or in any of the other elements except iron. Thus, the reason for this discrepancy is not clear. However, it is interesting to note that the measured intensity ratios between any two transitions from the $2s\,2p^4$ doublet levels in $_{22}$Ti XVI are in agreement with the calculated values.

As seen in Table III, agreement between the observed and calculated relative intensities of the observed lines in $_{26}$Fe XX is not within the error of the measurements. This is due to the fact that all of the observed lines in $_{26}$Fe XX are either blended or poorly separated from other iron lines; their brightnesses are therefore unreliable. Agreement between the observations and calculations in $_{28}$Ni XXII and $_{32}$Ge XXVI is good.

D. C I—like ions

The observed $2s^2 2p^2$-$2s\,2p^3$ transitions in the C I—like ions are listed in Table IV; the measured and calculated relative intensities are compared in Fig. 9. The C I—like ions have the most complex level structure of the F I— to B I—like ions. As a result, many transitions are observed, but they tend to be weaker, and are more often blended, than transitions in the simpler ions. Nevertheless, the C I—like ions are of particular interest because comparison of the observed and calculated relative intensities provides evidence that proton collisions within the ground configuration should be included in the level-population calculations.

The intensity ratio of two lines from $2s\,2p^3$ levels, one populated primarily from the ground $2s^2 2p^2\,^3P_0$ level and the other from an excited level in the $2s^2 2p^2$ configuration, such as $^3P_1$, $^3P_2$, or $^1D_2$, is predicted to be density sensitive.[11] As seen in Table IV, several of the line-intensity ratios in $_{22}$Ti XVII and $_{24}$Cr XIX are density dependent over the density range considered here and could therefore be used as density diagnostics. With the exceptions discussed below, agreement between the measured and calculated relative intensities is good.

The $^3D_3$ and $^3D_1$ levels in the $2s\,2p^3$ configuration are principally populated from the widely separated $2s^2 2p^2\,^3P_2$ and $2s^2 2p^2\,^3P_0$ levels, respectively. The proton-collisional rates between the latter two levels are larger than the corresponding electron rates;[11] as a result, the $^3P_0$-$^3D_1$ to $^3P_2$-$^3D_3$ intensity ratio can be used to determine the importance of including proton collisions in the calculations. In Table IV the relative intensity of the $^3P_0$-$^3D_1$ transition calculated[8] not including proton collisions is given in square brackets for $_{26}$Fe XXI, $_{28}$Ni XXIII, and $_{32}$Ge XXVII. Because the $2s^2 2p^2\,^3P_2$ and $2s^2 2p^2\,^3P_0$ levels separate rapidly with increasing Z, electron collisions become ineffective at coupling these levels in high-Z elements at the densities considered here. Thus, the difference between the two sets of values increases as Z increases and is large in $_{32}$Ge XXVII. It is clear that the measured values in $_{28}$Ni XXIII and $_{32}$Ge XXVII are in better agreement with the calculations including proton collisions than those not including proton collisions. In $_{32}$Ge XXVII the difference between the measured and calculated values including proton collisions is still significant. This is probably due to the fact that the proton-collisional rates depend on the ion temperature. The calculations assume an ion temperature equal to the electron temperature of maximum fractional abundance of the ion in coronal equilibrium; this value is probably incorrect for the plasmas considered here. In addition, proton-collisional rates calculated using the semiclassical technique may be too small. Note also that the calculations were made for protons whereas the observed plasmas were deuterium; however, the differences between the proton- and deuterium-collisional rates should be small, approximately a factor of $\sqrt{2}$. Nevertheless, this comparison indicates that proton collisions should be included in the calculations for the C I—like ions.

The measured and calculated values of the $^3P_1$-$^3S_1$ to $^3P_2$-$^3S_1$ branching ratio are in good agreement for $_{22}$Ti XVII at the high density and for $_{28}$Ni XXIII, but disagree in $_{22}$Ti XVII at the low density and in $_{26}$Fe XXI. The measured relative intensities of the $^3P_1$-$^3S_1$ and $^3P_2$-$^3S_1$ transitions in $_{28}$Ni XXIII and the $^3P_2$-$^3S_1$ transition

in $_{26}$Fe XXI relative to the intensity of the $^3P_2$-$^3D_3$ transition disagree with the calculations by almost a factor of 2. Agreement in the other elements is good; it is not clear whether this discrepancy is due to the measurements or the calculations.

The measured relative intensity of the $^1D_2$-$^1D_2$ transition is larger than the calculated value in $_{22}$Ti XVII at both densities and in $_{24}$Cr XIX at the high density (it was not observed in $_{24}$Cr XIX at the low density due to blending). According to the level-population calculations,[6,7] both lines are blended with relatively weak lines. Thus, the discrepancy does not appear to be due to the measurements; the population of the $2s^22p^2\,^1D_2$ level, the level from which the $2s2p^3\,^1D_2$ level is mainly populated, is larger than predicted by the calculations. The titanium and chromium level-population calculations include proton collisions; again, the reason for this disagreement is unclear.

E. B I—like ions

Table V lists the observed $2s^22p$-$2s2p^2$ transitions in the B I—like ions, and the measured and calculated relative intensities are compared in Fig. 10. These transitions tend to occur at longer wavelengths than those in the lower ionization states, an experimental advantage because most of the lines are unblended as a result. The reference transition, $^2P_{1/2}$-$^2S_{1/2}$, is strong and unblended in all the ions except for $_{26}$Fe XXII 117.17 Å, which is blended with $_{26}$Fe XXI 117.51 Å. However, the level-population calculations show that $_{26}$Fe XXI 117.51 Å is considerably weaker than $_{26}$Fe XXII 117.17 Å. Thus, this blend should not affect the accuracy of the relative intensities of the $_{26}$Fe XXII lines.

The $2s^22p$ configuration has two levels: the ground level $^2P_{1/2}$ and the excited level $^2P_{3/2}$. As the density increases to the value at which Boltzmann equilibrium between these levels is reached, the $^2P_{3/2}$ population increases relative to the $^2P_{1/2}$ population. As a result, the intensity ratio of a line from one of the $2s2p^2$ levels, $^2P_{1/2}$, $^2S_{1/2}$, or $^2D_{3/2}$, which are primarily populated from the $2s^22p\,^2P_{1/2}$ level, with a line from the $2s2p^2\,^2P_{3/2}$ or $2s2p^2\,^2D_{5/2}$ level, which receive their populations principally from the $2s^22p\,^2P_{3/2}$ level, is expected to be density dependent.[10] This is demonstrated by the $_{22}$Ti XVIII and $_{24}$Cr XX data presented in Table V.

With two exceptions, agreement between the measured and calculated relative intensities at the high density is good. The measured relative intensity of the $_{26}$Fe XXII 135.78-Å line is smaller than the predicted value by almost a factor of 2; this was also observed by Stratton, Moos, and Finkenthal[2] at a density of 5×10^{12} cm^{-3}, although agreement between the measured and calculated values at a density of 3.5×10^{13} cm^{-3} was good. The measured relative intensity of the $_{28}$Ni XXIV 138.80-Å line is larger than the calculated value by a factor of 2. Agreement between the measured and calculated relative intensities of the same transition, $^2P_{3/2}$-$^2D_{5/2}$, in $_{22}$Ti XVIII and $_{26}$Fe XXII is good, and so the measured relative intensity of the $_{28}$Ni XXIV 138.80-Å line is too large; the line is very weak (see Fig. 4), and so its brightness is unreliable.

At the lower density, several discrepancies between the measured and calculated relative intensities are found: In $_{22}$Ti XVIII the 147.58- and 179.87-Å lines are almost a factor of 2 weaker than predicted, and in $_{24}$Cr XX the 128.42-Å line is brighter than predicted by more than a factor of 2. In the last case the disagreement is probably due to the blending of the $_{24}$Cr XX 128.42-Å line with the $_{24}$Cr XVIII 128.10-Å line. The $_{22}$Ti XVIII 147.58-Å line is poorly separated from the $_{22}$Ti XVIII 148.52-Å line, making its brightness unreliable. The reason for the discrepancy in the case of the $_{22}$Ti XVIII 179.87-Å line is unclear. Note, however, that the $2s2p^2\,^2P_{1/2}$ and $2s2p^2\,^2S_{1/2}$ levels cross near $_{23}$V XIX;[20] this may affect the accuracy of the calculated transition probabilities for some transitions departing from these levels in $_{22}$Ti XVIII and $_{24}$Cr XX.

V. SUMMARY

Of the 58 lines observed at the high density, the measured relative intensities of 47 agree with the predicted values within 30%, the estimated accuracy of the measurements. (These totals do not include the reference lines but do include the branching ratios.) In most cases the exceptions can be reasonably attributed to problems with the measurements. Only for the following lines is the reason for the disagreement between the measured and calculated relative intensities unclear: $2s^22p^2\,^3P_1$—$2s2p^3\,^3S_1$ in $_{28}$Ni XXIII, $2s^22p^2\,^3P_2$—$2s2p^3\,^3S_1$ in $_{26}$Fe XXI and $_{28}$Ni XXIII, and $2s^22p^2\,^2D_{3/2}$ in $_{26}$Fe XXII. In the C I—like ions there is evidence that proton collisions play an important role in determining the level populations in the ground configuration and should therefore be included in the level-population calculations for these ions.

At the low density, agreement between the measured and calculated relative intensities is not as good: The measured relative intensities of only 16 out of the 33 observed lines agree with the calculated values within 30%. Again, the exceptions can be traced to problems with the measurements in most cases. The cases in which unexplained disagreement between the calculated and measured relative intensities is significantly greater than 30% are the following: $2s^22p^3\,^2D_{5/2}$—$2s2p^4\,^2P_{3/2}$, $2s^22p^3\,^2D_{3/2}$—$2s2p^4\,^2D_{3/2}$, and $2s^22p^3\,^2D_{5/2}$—$2s2p^4\,^2D_{5/2}$ in $_{22}$Ti XVI; $2s^22p^2\,^3P_1$—$2s2p^3\,^3S_1$, $2s^22p^2\,^3P_2$—$2s2p^3\,^3S_1$, and $2s^22p^2\,^1D_2$—$2s2p^3\,^1D_2$ in $_{22}$Ti XVII; and $2s^22p\,^2P_{1/2}$—$2s2p^2\,^2D_{3/2}$ in $_{22}$Ti XVIII.

There are several ways in which this work can be improved and extended. Comparison of measured and calculated line-intensity ratios at a number of densities, instead of just two, would provide a more precise determination of the reliability of the ratios for density diagnostics, as well as a more rigorous test of the level-population calculations. It is of particular interest to compare measured and calculated line-intensity ratios in which one of the lines is due to an allowed transition and the other line is due to a forbidden transition within the ground configuration. Such ratios can be more strongly density dependent than ratios of two allowed transitions and are therefore well suited to density diagnostics. Understanding of the relative intensities of the forbidden

transitions would also allow them to be used for other diagnostic purposes, such as measurement of impurity densities. The forbidden transitions occur at longer wavelengths than the allowed transitions, with many above 1000 Å; additional instrumentation would therefore be required for these measurements. Finally, higher-resolution measurements would increase the number of lines available for comparison by reducing the number of blends.

In conclusion, it appears that the level-population calculations may be used with some confidence for spectroscopic plasma diagnostics. However, additional study is needed to determine the causes of the discrepancies between the calculations and measurements discussed above.

ACKNOWLEDGMENTS

The authors would like to thank the PLT group, in particular, J. Hosea, P. Colestock, D. Hwang, J. Strachan, and J. R. Wilson for supporting these measurements; S. Cohen, J. Timberlake, and T. Bennett for providing the impurity injection; and M. Finkenthal of the Hebrew University (Jerusalem) for useful discussions. This work was supported by the U.S. Department of Energy under Contracts No. DE-AS02-76ET53006 (The Johns Hopkins University), No. DE-AI05-83ER53145 (The Naval Research Laboratory), and No. DE-AC02-76CH03073 (The Princeton Plasma Physics Laboratory).

---

*Present address: Plasma Physics Laboratory, Princeton University, Princeton, NJ 08544.

[1]S. Suckewer and E. Hinnov, Phys. Rev. A **20**, 518 (1979).
[2]B. C. Stratton, H. W. Moss, and M. Finkenthal, Ap. J. Lett. **279**, L31 (1984).
[3]E. Hinnov, Ap. J. Lett. **230**, L197 (1979).
[4]C. Breton, C. DeMichelis, M. Finkenthal, and M. Mattioli, J. Opt. Soc. Am. **69**, 1652 (1979).
[5]S. O. Kastner, W. M. Neupert, and M. Swartz, Ap. J. **191**, 261 (1974).
[6]A. K. Bhatia, U. Feldman, and G. A. Doschek, J. Appl. Phys. **51**, 1464 (1980).
[7]U. Feldman, G. A. Doschek, C. C. Cheng, and A. K. Bhatia, J. Appl. Phys. **51**, 190 (1980).
[8]U. Feldman, J. F. Seely, and A. K. Bhatia, At. Data Nucl. Data Tables (to be published).
[9]H. E. Mason and A. K. Bhatia, Astron. Astrophys. Suppl. Ser. **52**, 181 (1983).
[10]H. E. Mason and P. J. Storey, Mon. Not. R. Astron. Soc. **191**, 631 (1980).
[11]H. E. Mason, G. A. Doschek, U. Feldman, and A. K. Bhatia, Astron. Astrophys. **73**, 74 (1979).
[12]U. Feldman, G. A. Doschek, and A. K. Bhatia, J. Appl. Phys. **53**, 8554 (1982).
[13]S. Suckewer, Phys. Rev. **170**, 239 (1968).
[14]S. Suckewer, J. Phys. B **3**, 380 (1970); **3**, 390 (1970).
[15]U. Feldman and G. A. Doschek, J. Opt. Soc. Am. **67**, 726 (1977).
[16]D. Hwang *et al.*, in *Plasma Physics and Controlled Nuclear Fusion Research,* Proceedings of the 9th International Conference, Baltimore, 1982 (IAEA, Vienna, 1983), Vol. 3, p. 3.
[17]W. L. Hodge, B. C. Stratton, and H. W. Moos, Rev. Sci. Instrum. **55**, 16 (1984).
[18]E. Marmar, J. Cecchi, and S. Cohen, Rev. Sci. Instrum. **46**, 1149 (1975).
[19]S. Cohen *et al.*, J. Vac. Sci. Technol. **20**, 1226 (1982).
[20]K. D. Lawson, N. J. Peacock, and M. F. Stamp, J. Phys. B **14**, 1929 (1981).
[21]B. Edlén, Phys. Scr. **22**, 593 (1981).
[22]B. Edlén, Phys. Scr. **28**, 51 (1983).
[23]W. E. Behring, J. F. Seely, Samuel Goldsmith, Leonard Cohen, M. Richardson, and U. Feldman, J. Opt. Soc. Am. B (to be published).
[24]B. Edlén, Phys. Scr. **28**, 483 (1983).
[25]K. T. Cheng, Y. K. Kim, and J. P. Desclaux, At. Data Nucl. Data Tables **24**, 111 (1979).